Progress in Natural Science: Materials International 28 (2018) 160–167

HOSTED BY

Contents lists available at ScienceDirect

Progress in Natural Science: Materials International

journal homepage: www.elsevier.com/locate/pnsmi

Original Research

Effects of -NO_2 and -NH_2 functional groups in mixed-linker Zr-based MOFs on gas adsorption of CO_2 and CH_4

Zana Hassan Rada[a], Hussein Rasool Abid[a,b], Hongqi Sun[c], Jin Shang[d], Jiaye Li[e], Yingdian He[f], Shaomin Liu[a], Shaobin Wang[a,*]

[a] Department of Chemical Engineering, Curtin University, GPO Box U1987, Perth, WA 6845, Australia
[b] Department of Environmental Health, Applied Medical Science College, Karbala University, Iraq
[c] School of Engineering, Edith Cowan University, Joondalup, WA 6027, Australia
[d] School of Energy and Environment, City University of Hong Kong, Tat Chee Avenue, Kowloon, Hong Kong, China
[e] Department of Chemistry, Monash University, Victoria 3800, Australia
[f] Department of Chemical and Biomolecular Engineering, The University of Melbourne, Victoria 3010, Australia

ARTICLE INFO

Keywords:
UiO-66–NO_2
UiO-66-NH_2
Multi-linker MOFs
Carbon dioxide
Methane adsorption

ABSTRACT

This study was undertaken to evaluate the effects of mixing BDC-NO_2 and BDC-NH_2 linkers in the synthesis of Zr-based metal organic frameworks (Zr-MOFs) on their adsorption and separation of CO_2 and CH_4. UiO-66 with single or binary -NO_2 and -NH_2 samples were synthesized under solvothermal conditions and activated by solvent exchanging using methanol. Structural analyses of the materials were conducted using FTIR, XRD, TGA, SEM, ^{1}HNMR and N_2 adsorption/desorption techniques and adsorption of CO_2 and CH_4 at high pressures and different temperatures (273 and 298 K) was investigated. It was found that UiO-66-NH_2 exhibited higher CO_2 and CH_4 adsorption capacities than those of UiO-66-NO_2. Addition of -NH_2 functional group in UiO-66-NO_2 could enhance CO_2 and CH_4 adsorption due to the extra CO_2 adsorption sites of -NH_2 functional groups. Addition of -NO_2 functional group to UiO-66-NH_2 at a low loading could also increase CO_2 and CH_4 adsorption, however, a high loading of NO_2 functional group to UiO-66-NH_2 would result in decreased adsorption.

1. Introduction

Capture and separation of carbon dioxide from methane is one of major process for high-valued methane utilization. The effective separation of carbon dioxide (CO_2) from methane (CH_4) can be achieved through some technologies. Adsorption based separation technology such as physical adsorption by porous materials is considered to be a cost efficient process and many types of adsorbent materials have been examined, such as activated carbon, zeolites and metal organic frameworks (MOFs) [1–8].

Metal organic frameworks (MOFs) are a new class of crystalline and promising porous materials, which have recently attracted considerable interest in many applications for gas adsorption and storage, due to their high specific surface area and pore volume. Until now, numerous MOFs have been synthesized and studied in capture of CO_2, storage of CH_4 and their separation [9,10]. Mg-MOF-74, zeolitic imidazolate frameworks (ZIFs) and bio-MOF-11 have showed high CO_2 adsorption [11–13]. For methane storage, Ni-MOF-74 [14–16], MOF-177 [17] and PCN-14 [18] have been demonstrated good capacities.

The uptake capacities of CO_2 and CH_4 on MOFs are dependent on the structural properties such as pore volume and surface area of MOFs. However, achieving a highly selective uptake of a specific gas on MOFs, a balanced porosity and functionality of the framework should be considered [10]. In addition, different types of functional groups (Br, CH_3, NO_2, NH_2, etc.) in the structure of MOFs [19,20] also affect the surface area and adsorption. Ying et al. stated that NH_2 group can show a good role and provide strong affinity for CO_2 molecules in the adsorption [21]. And NO_2 group can also play as Lewis basic sites to increase CO_2 adsorption by acid-base interactions [22].

Many functionalized MOFs [23] have been shown as good adsorbents for CO_2 and CH_4 uptakes [24–26]. Amino (NH_2)-functionalized MOFs usually displayed an improvement in separation of CO_2/CH_4 [27,28] whereas nitro (NO_2) functionalized MOFs reduced surface area and CO_2/CH_4 adsorption [29].

Recently, combination of two different ligands (functional group or non-functional group) over MOFs have been studied by some researchers [30]. The MOFs were referred as mixed linker MOFs (Mix-MOFs). The properties of MixMOFs led them to be promising sorbent

Peer review under responsibility of Chinese Materials Research Society.
* Corresponding author.
E-mail address: shaobin.wang@curtin.edu.au (S. Wang).

https://doi.org/10.1016/j.pnsc.2018.01.016
Received 13 November 2017; Accepted 2 January 2018
Available online 13 March 2018

materials for CO_2 and CH_4 adsorption, such as Al-MIL-53, CAU-10 [31], Ti-based MOFs [32] and UiO-66 [33] mixed linker MOFs. More recently, UiO-66 mixed linker MOFs have been studied by two research groups due to their high thermal and chemical stabilities. Kim et al. [34] synthesized a mixture of BDC-NH_2 and Br-BDC functionalized UiO-66-Br-NH_2. A mixture of BDC (non-functional linker) with BDC-NH_2 at different loadings functionalized UiO-66 has been studied by Chavan et al. [33].

In this article, for the first time, BDC-NO_2 and BDC-NH_2 functionalized linkers at different loadings were used for preparation of MixMOFs of UiO-66 and their physicochemical properties and performances in CO_2 and CH_4 adsorption were characterized and compared with single functionalized UiO-66-NO_2 and UiO-66-NH_2.

2. Experimental section

2.1. Chemicals and synthesis of different UiO-66 samples

All chemicals including zirconium chloride ($ZrCl_4$, 99.9%), N, N-dimethylformamide (DMF, C_3H_7NO, 98%), methanol (CH_3OH, 99%), 2-nitroterephthalic acid (BDC-NO_2, ≥ 99%), and 2-aminoterephthalic acids (BDC-NH_2, 99%) were supplied by Sigma–Aldrich without further purification.

UiO-66-NO_2 was synthesized based on the previous reports [35]. In a typical process, $ZrCl_4$ (6.5 mmol) was dissolved in DMF (86 mL) in a Teflon vessel and stirred for 10 min. BDC-NO_2 (6 mmole) was then added to the solution and stirred for 20 min. The homogeneous mixture was placed in a Parr PTFE-lined digestion vessel of 125 mL, sealed and left in an oven for 24 h at 393 K. The product was washed two times with DMF and filtered by vacuum filtration. UiO-66-NH_2 was obtained by the similar synthesis procedure of UiO-66-NO_2 using a BDC-NH_2 linker instead of BDC-NO_2.

Synthesis of mixed linker UiO-66-NO_2-N (N = NH_2) and UiO-66-NH_2-N (N = NO_2) were achieved by using the above process through different ratios of the two linkers, BDC-NO_2 and BDC-NH_2 as described in Table S1 (ESI). The molar fractions of BDC-NH_2 with respect to BDC-NO_2 were at 0.10 and 0.75 for UiO-66-NO_2-N samples and vice versa for UiO-66-NH_2-N samples, and the linker BDC-NO_2 with respect to BDC-NH_2 were also at 0.10 and 0.75.

Activation of all samples were carried out using the method as previously reported [35]. About 0.5 g of each sample was immersed separately in 50 mL of methanol solution for 5 d and then the solids were filtered and dried in an oven at 353 K for 12 h. Finally, these materials were heated under vacuum at 463 K overnight.

2.2. Characterization of samples

The crystalline structure of samples was confirmed by a XRD diffractometer (D8 Advance-diffractometer Bruker XS) with Cu Kα radiation (λ = 1.5406 Å). A FTIR spectrometer (Perkin-Elmer 100 FT-IR spectrometer) was used to investigate functional groups on MOF crystalline structure. The spectrum was scanned from 600 to 4000 cm^{-1} with a resolution of 4 cm^{-1} by using an attenuated total reflectance (ATR) technique. Thermal stabilities of all samples were investigated by using a thermogravimetric analysis (TGA) instrument (TGA/DSC1 STAR^e system, METTLER-TOLEDO). About 10–20 mg samples were loaded in an alumina pan and then argon gas was introduced into the furnace at a flow rate of 20 mL/min and a heating rate of 10 K/min from 308 to 1150 K. A SEM machine (Zeiss NEON 40 EsB Cross-Beam) was used to determine the morphologies of the samples. Surface area and pore size of each sample were measured by a Micromeritics Tristar 3000 analyzer. All samples were degassed at 463 K under vacuum overnight and then N_2 adsorption at 77 K was carried out. ^{1}HNMR spectroscopy was used to detect the incorporation of the linkers BDC-NO_2 and BDC-NH_2 into MOF samples. About 20 mg of samples were digested in 600 μL of NaOH-D_2O solution for 24 h before the measurement. The data were recorded on a Bruker Advance III 400 spectrometer and were indirectly referenced to TMS using the resonance of the residual solvent peak.

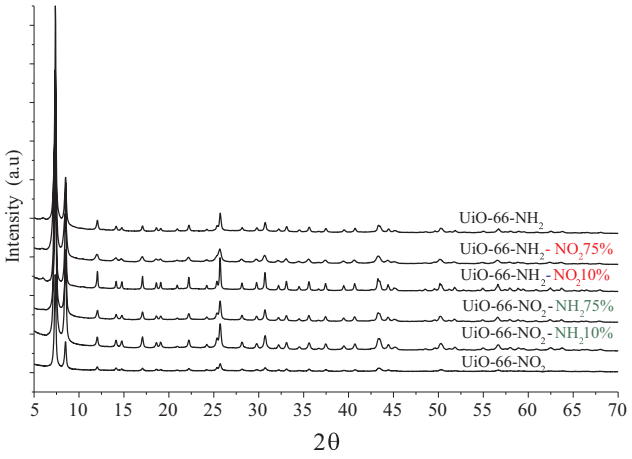

Fig. 1. XRD patterns of as-synthesized UiO-66-NO_2-N, UiO-66-NH_2-N, UiO-66-NO_2 and UiO-66-NH_2 samples.

2.3. Adsorption study of CO_2 and CH_4

A Micromeritics-ASAP2050 was used to measure the adsorption isotherms of pure CO_2 (99.995%) and CH_4 (99.995%) at high pressure up to 1000 kPa on samples. Carbon dioxide (99.995%) and methane (99.995%) were supplied by Coregas. First, the samples were thoroughly dehydrated and degassed on the Micromeritics ASAP2050 analyzer by heating stepwise at 1 K/min up to 423 K and holding at this temperature for 8 h under high vacuum. An equilibrium interval of 20 s was adopted in all the isotherm measurements. The adsorption was carried out at temperatures of both 273 and 298 K.

3. Results and discussion

Fig. 1 shows XRD patterns of prepared mixed linker UiO-66-NO_2-N (N = NH_2) and UiO-66-NH_2-N (N = NO_2) with pure UiO-66-NO_2 and UiO-66-NH_2. The profiles of the as-synthesized samples clearly show that the crystalline structures of mixed linker samples are matching to single linker UiO-66-NO_2 and UiO-66-NH_2 as reported in the previous study [36–38]. Fig. S1 (ESI) presented all samples after methanol activation. It was found that methanol activation did not affect the crystalline structures of all samples.

Figs. 2 and 3 show FTIR spectra of non-activated and activated

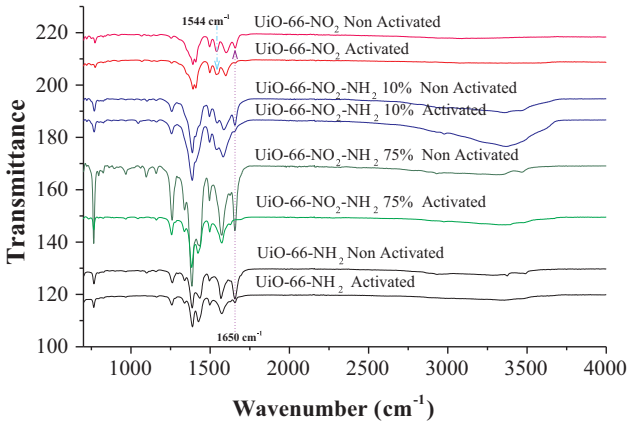

Fig. 2. Comparison of FTIR spectra of mixed linker UiO-66-NO_2-N, UiO-66-NO_2 and UiO-66-NH_2 samples.

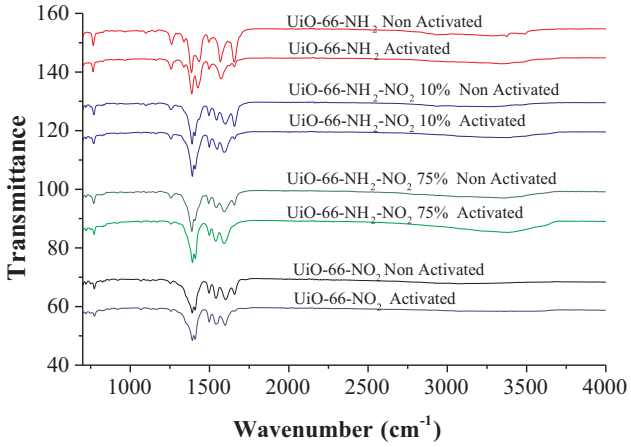

Fig. 3. Comparison of FTIR spectra of mixed linker UiO-66-NH_2-N, UiO-66-NO_2-N, UiO-66-NO_2, and UiO-66-NH_2 samples.

samples. The functional carboxyl in free aromatic carboxylic acid on non-activated samples was observed at 1650 cm^{-1}. However, after activation of the samples by methanol, the peak was mostly disappeared, demonstrating that a good exchange of DMF by methanol. [39] The asymmetric ($\nu(NO)_{asym}$) peak at 1544 cm^{-1} reduced and disappeared at loading of 10% and 75% (-NH_2) group to UiO-66-NO_2, meanwhile the C-N stretching of aromatic amines appeared at 1356 cm^{-1} on both the samples of UiO-66-NO_2-NH_2 − 10% and UiO-66-NO_2-NH_2 − 75% [33]. In contrast, the asymmetric ($\nu(NO)_{asym}$) vibration at 1544 cm^{-1} appeared on mixed linker samples and the C-N stretching of aromatic amines at 1356 cm^{-1} was missing at the loading 10% and 75% of (-NO_2) group to UiO-66-NH_2 samples. A similar behavior was observed for the symmetric ($\nu(NO)_{sym}$) stretching at 1355 cm^{-1}, which decreased after loading the UiO-66-NO_2 sample with (-NH_2) group and vice versa with the addition of (-NO_2) groups to the sample UiO-66-NH_2 [40,41].

The ^{1}H NMR spectra of synthesized samples are shown in Fig. 4. As it can be seen that, BDC-NH_2 and BDC-NO_2 linkers can be found in UiO-66-NH_2 and UiO-66-NO_2, respectively [38]. For the mixed-linker UiO-66-NO_2-NH_2, both BDC-NH_2 and BDC-NO_2 linkers were found. As expected, by increasing the amount of BDC-NH_2 linker into UiO-66-NO_2 sample, the signals of BDC-NH_2 become more visible in samples of UiO-66-NO_2-NH_2 10% and UiO-66-NO_2-NH_2 75% and vice versa with increased BDC-NO_2 linkers to UiO-66-NH_2 samples. The intensities of BDC-NO_2 signals in UiO-66-NH_2-NO_2 10% and UiO-66-NH_2-NO_2 75% samples were obviously presented. Thus, ^{1}H NMR spectra clearly proved the incorporation of the linkers into the frameworks of the samples.

The thermal stability of samples was examined by TGA and weight loss profiles are presented in Fig. 5. DTG profiles of all samples are illustrated in Fig. S3. The TGA curves of non-activated samples showed three-steps of weight losses. The first step of the weight loss at 5 − 8% occurred from 305 to 375 K and it is attributed to the removal of moisture and free solvent inside the pores [42]. Meanwhile, the second weight loss at 23 − 30% took place in the range of 375–460 K and this loss is related to the removal of un-coordinated linkers and coordinated solvent (DMF), due to the strong chemical bonding. The last stage (third-step) of weight loss at 62 − 72% is referred to the structural collapse of the MOF samples occurring at 760 K. Fig. 5(b) shows the TGA results for activated samples. It can be confirmed that weight losses appear on all samples with slight differences in the non-activated samples. The removal of moisture and free solvent (initial step) happened at 350 K with 12 − 22% weight loss. However, the second step of weight loss on activated samples presented very small amount of 5% loss compared with the non-activated samples. This provides the evidence of successful exchange of the solvent [33]. The decomposition temperature of activated samples slightly increased to 820 K, suggesting their higher thermal stability.

Fig. 6 presents N_2 adsorption/desorption isotherms at 77 K. A different hysteresis was observed in all samples, which indicates the presence of mesoporous structure with the micropores. A similar observation on functionalized UiO-66 samples has been reported previously [33]. The BET surface areas, micropore volumes and areas of the samples by the t-plot method are presented in Table S2 (ESI). The surface areas can be increased at the lower loading of a second linker but declined with further increasing loading of the functional linkers to UiO-66-NH_2 or UiO-66-NO_2 samples. UiO-66-NO_2-NH_2 10% and UiO-66-NH_2-NO_2 10% displayed higher surface areas at 867 m^2g^{-1} and

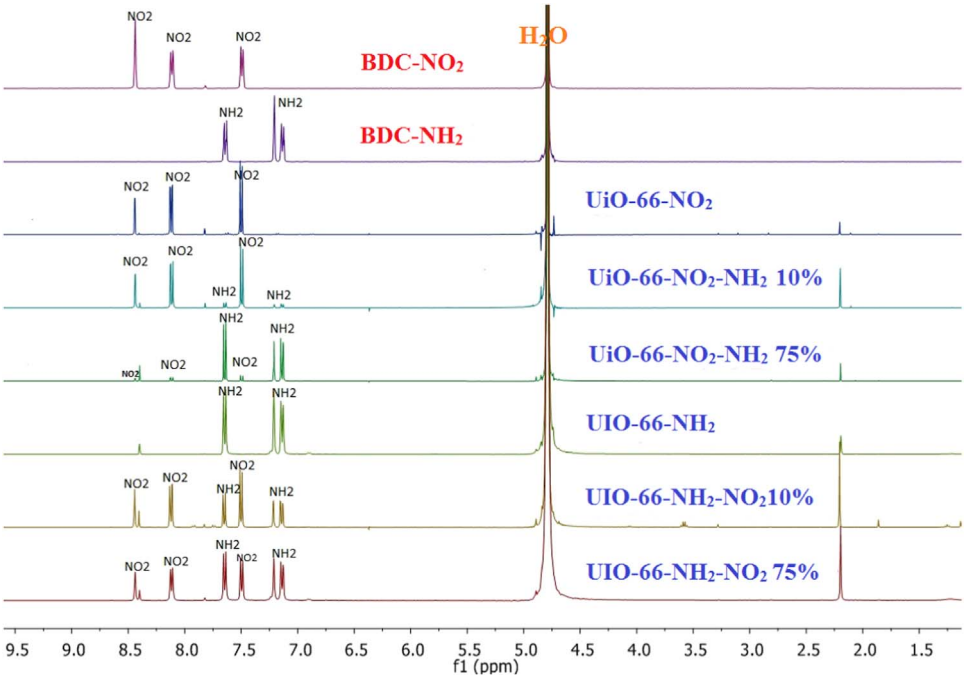

Fig. 4. ^{1}H NMR spectra of linkers BDC-NO_2 and BDC-NH_2 in prepared MOFs samples.

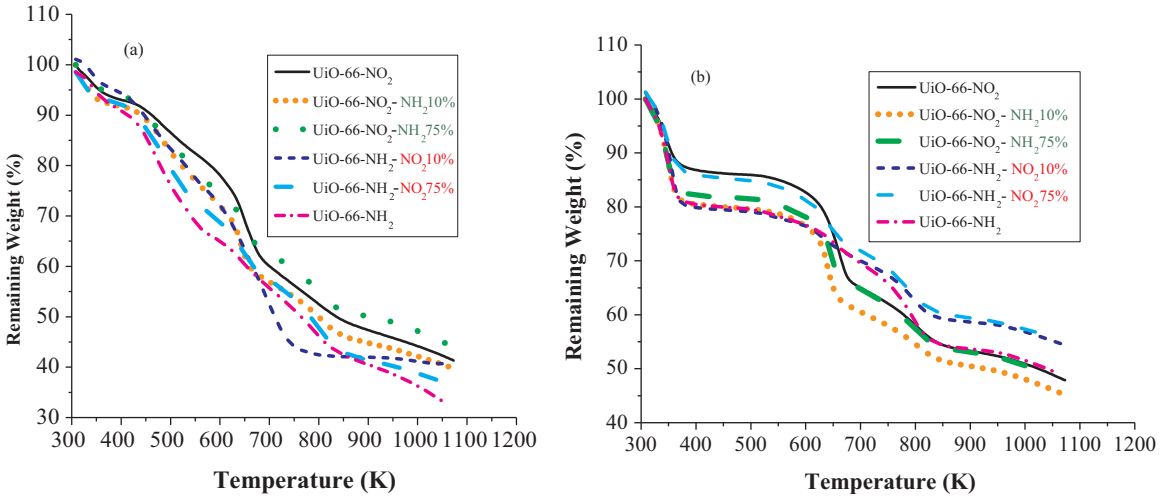

Fig. 5. TGA profiles of UiO-66-NO_2-N, UiO-66-NH_2-N, UiO-66-NO_2 and UiO-66-NH_2 samples (a) before activation (b) after activation.

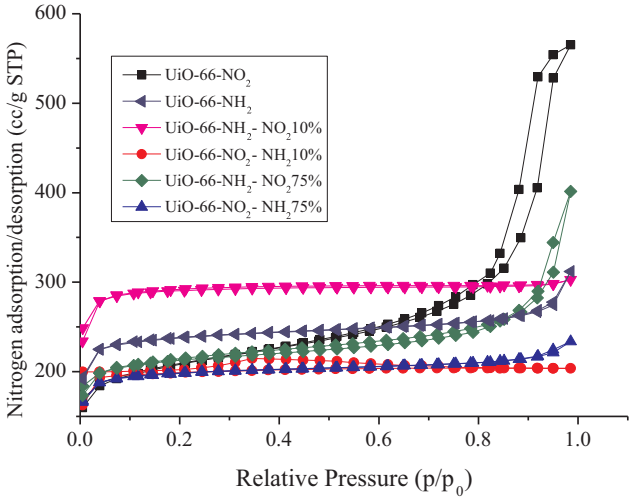

Fig. 6. N_2 adsorption/desorption isotherms on the UiO-66 samples.

1152 m^2g^{-1} than single linker functionalized samples, UiO-66-NO_2 and UiO-66-NH_2 at 771 m^2g^{-1} and 1025 m^2g^{-1}, respectively. More specifically, BDC-NO_2 linker has the least favorable energy of structural assembly because of the electronegative -NO_2 group. Adding few amount of BDC-NH_2 linker may enhance the formation of the structure of UiO-66-NO_2 and enhance the specific surface area as demonstrated in UiO-66-NO_2-NH_2. On the other hand, NH_2-linker segregates itself from others because this linker can build hydrogen bonds with both BDC-NH_2 itself and the solvent [43]. Therefore, adding few amount of BDC-NO_2 linker may attenuate the hydrogen bond insides the pores and at the same time enhance the microporosity of the materials, leading to the increase in the specific surface area as observed in UiO-66-NH_2-NO_2 10% [44,45].

However, the pore sizes of UiO-66-NO_2-NH_2 10% and UiO-66-NH_2-NO_2 10% samples were significantly decreased.

SEM pictures of samples are presented in Fig. 7. All samples exhibit a similar crystalline morphology of Zr-MOFs reported before [37,46,47] with homogeneous triangular base-pyramid particles at different sizes. UiO-66-NO_2 was obtained as a smaller crystal size and aggregated crystals, however, modified samples present a larger particle size than single functionalized samples. In addition, with loading of BDC-NO_2 and BDC-NH_2 linkers into single linker MOFs samples, the size of the crystals increased and became less aggregated that may be related to different polarities of the ligands [48].

Figs. 8 and 9 show CO_2 and CH_4 adsorption isotherms on all samples at varying temperatures (273 and 296 K). In general, all samples exposed affinity to adsorb CO_2 higher than CH_4. Furthermore, UiO-66-NH_2 presented higher capacities than UiO-66-NO_2 to adsorb both CO_2 and CH_4. The presences of BDC-NH_2 as a second linker at different ratios of 10% and 75% increased CO_2 and CH_4 adsorption. UiO-66-NO_2-NH_2 10% and UiO-66-NO_2-NH_2 75% showed the values of CO_2 uptakes at 4.96 and 4.31 mmol/g at 298 K, respectively, and the adsorption capacities were at 6.33 and 6.00 mmol/g at 273 K, respectively. The amounts of CH_4 uptake were 2.04 and 1.90 mmol/g at 298 K and they were higher at 2.9 and 2.76 mmol/g at 273 K for UiO-66-NO_2-NH_2 10% and UiO-66-NO_2-NH_2 75%, respectively. The high surface area and the presence of amino functional groups can increase the affinity towards the gas uptakes [49] (CO_2 and CH4) on mixed ligand samples. It seems that the adsorption of CO_2 and CH_4 on the bifunctional UiO-66 samples in this study is higher than that of several other MOFs such as FMOF-2, MIL-20, MIL-125(Ti), ZIF-100 and ZIF-95. However, MIL-53(Cr) and Zeolite 13× presented higher capacities than the samples reported here, as shown in Table 1.

However, loading 10% and 75% of BDC-NO_2 group on UiO-66-NH_2 shows slightly different effects on CO_2 and CH_4 adsorption. Mixed UiO-66-NH_2-NO_2 10% showed higher CO_2 and CH_4 uptakes than those of single UiO-66-NH_2, meanwhile, UiO-66-NH_2-NO_2 75% presented less values of CO_2 and CH_4 adsorption than UiO-66-NH_2. High interconnection between the linkers leads to decrease of the surface area of UiO-66-NH_2-NO_2 75% compared with UiO-66-NH_2-NO_2 10% and UiO-66-NH_2. In contrast, the surface area and porosity of UiO-66-NH_2-NO_2 10% are increased. Adding a small amount of BDC-NO_2 group can enhance the affinity of the structure toward CO_2 with less interconnection between the linkers. In addition, BDC-NO_2 group within the structure may lead to increase the polarity of the linker by changing the charge distribution toward CH_4 and CO_2 adsorption. The highly polar -NO_2 groups with the negative charge density on O atoms may interact with the Lewis acidic C center of CO_2 molecules on the basis of the dipole−quadruple interaction [56]. The quadrupole moment of CO_2 (-13.4×10^{-40} C. m^2) creates strong interactions with adsorbents. Suitable sizes of micropores within MOF structure also affect CH_4 molecular adsorption [57].

The selectivity of CO_2 over CH_4 by the static adsorption at pressure up to 1000 kPa was calculated according to Eq. S1 and displayed in Fig. 10. UiO-66-NH_2 gave a better selectivity than UiO-66-NO_2. Addition of a second linker BDC–NO_2 to UiO-66-NH_2 improves the selectivity while addition of BDC-NH_2 to UiO-66-NO_2 can result in a lower selectivity because the electron withdrawing nature of the nitro group would be expected to strongly impact coordination where the nitro

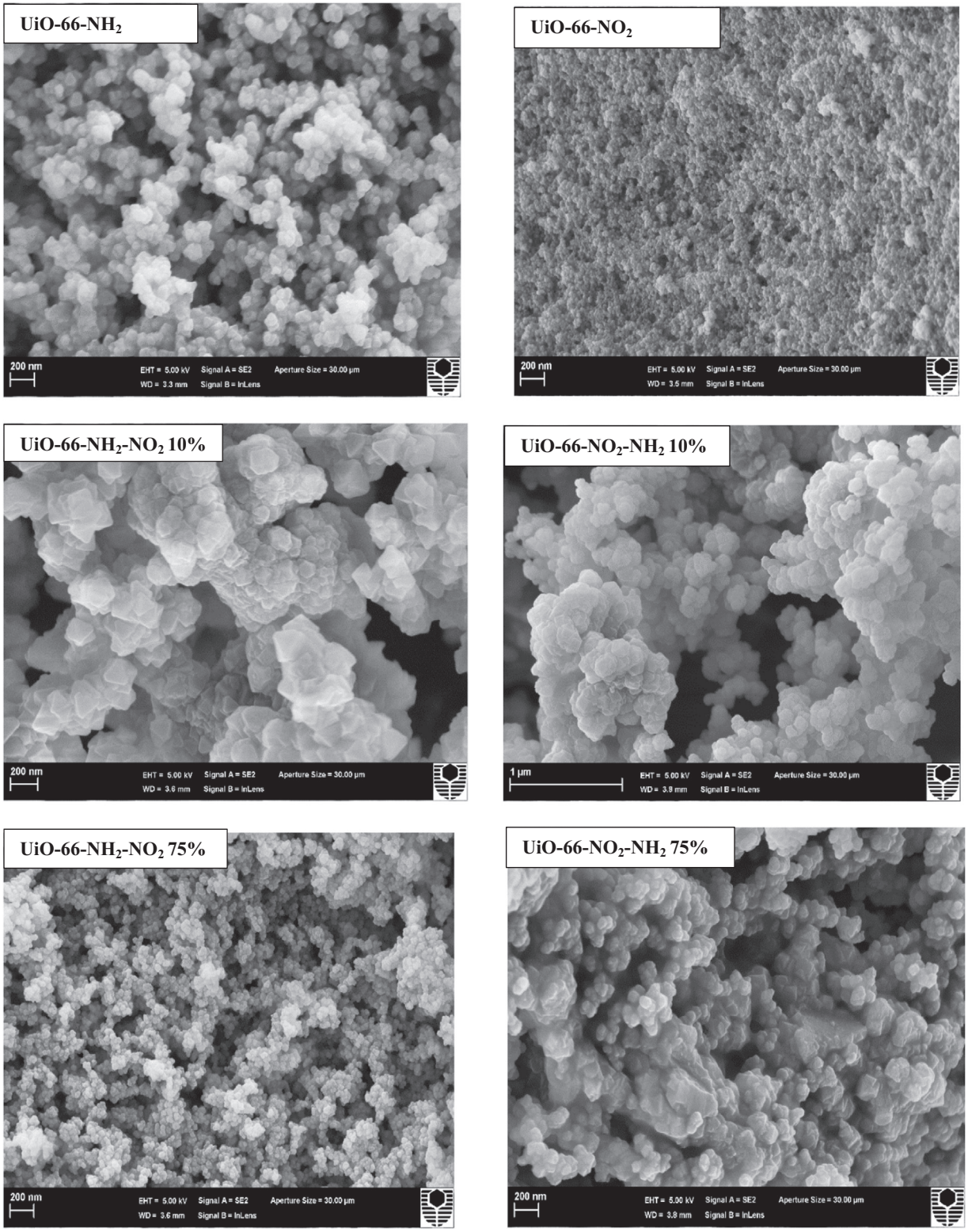

Fig. 7. SEM images of synthesized UiO-66 samples.

group affected the sorption of protic guests [58]. Consequently, the N-based Lewis basic functional polar surfaces in the framework may also lead to the high CO_2 selectivity [56]. At pressure of 1000 kPa, UiO-66-NO_2-NH_2 75% has the lowest separation factor for carbon dioxide over methane (2.05) and (2.16) at 298 K and 273 K, respectively, whereas, UiO-66-NH_2-NO_2 10% displays the best selectivity amongst others. The selectivity of CO_2 over CH_4 decreased with increasing pressure. Therefore, the selectivity of CO_2 /CH_4 of most samples at pressure lower than 200 kPs can be selected as best separation. Table 2 summarizes the selectivity of CO_2 over CH_4 on various MOFs. The selectivities of CO_2 over CH_4 for mixed ligands MOFs are better in comparison with other MOFs.

In Figs. S4 and S5 (ESI), the isosteric heats of adsorption (Q_{st}) for CO_2 and CH_4 were determined based on the Clausius–Claperyron

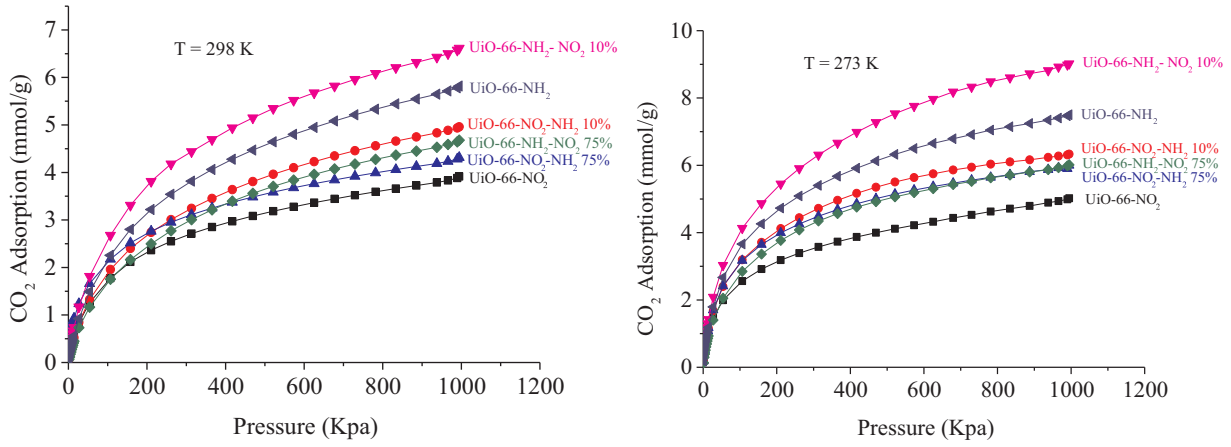

Fig. 8. CO_2 adsorption on UiO-66-NO_2, UiO-66-NO_2-N, UiO-66-NH_2-N and UiO-66-NH_2 samples at different temperatures.

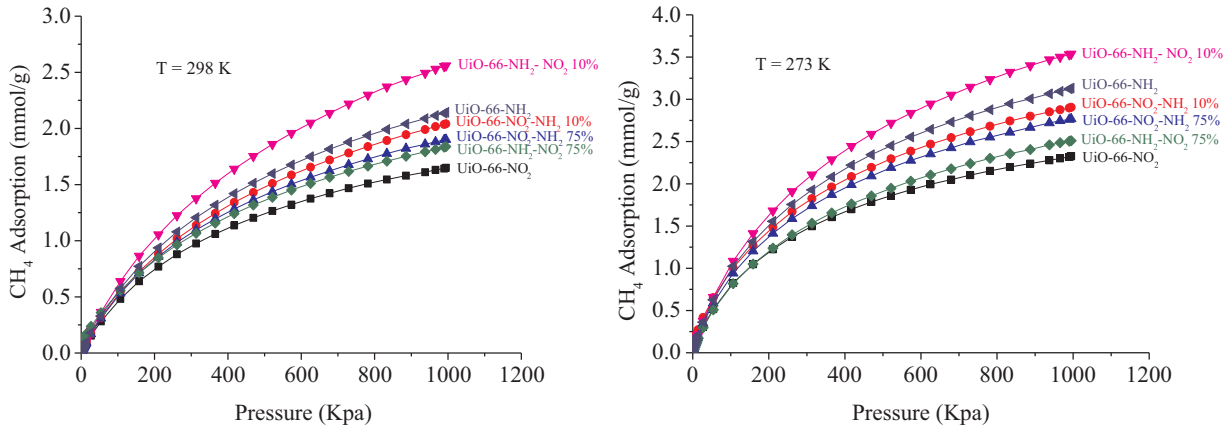

Fig. 9. CH_4 adsorption on UiO-66-NO_2, UiO-66-NO_2-N, UiO-66-NH_2-N and UiO-66-NH_2 samples at different temperatures.

Table 1
Comparison of CH_4 and CO_2 adsorption on various materials.

MOFs	CO_2 adsorption (mmol/g)	CH_4 adsorption (mmol/g)	References
ZIF−95	0.9 (273 K, 1 bar)	0.3 (273 K, 1 bar)	[50]
ZIF−100	1.1 (273 K, 1 bar)	0.31(273 K, 1 bar)	[50]
MIL−125(Ti)	4.28(273 K, 9.8 bar)	1.46 (273k, 9.8 bar)	[51]
MIL−120	4.8 (303 K, 10 bar)	1.8 (303 K, 10 bar)	[52]
FMOF−2	5.1 (298 K, 30 bar)	1.3 (298 K, 30 bar)	[53]
Zeolite 13×	7.72 (273 K)	4.02 (273 K)	[54]
MIL−53(Cr)	8 (304 K, 10 bar)	3.7 (304 K, 10 bar)	[55]
UiO−66-NH_2	7.5 (273 K, 9.8 bar)	3.1 (273 K, 9.8 bar)	This work
UiO−66-NH_2-NO_2 10%	9.0 (273 K, 9.8 bar)	3.5 (273 K, 9.8 bar)	This work
UiO−66-NH_2-NO_2 75%	6.0 (273 K, 9.8 bar)	2.5 (273 K, 9.8 bar)	This work
UiO−66-NO_2-NH_2 75%	6.0 (273 K, 9.8 bar)	2.7 (273 K, 9.8 bar)	This work
UiO−66-NO_2-NH_2 10%	6.3 (273 K, 9.8 bar)	2.8 (273 K, 9.8 bar)	This work
UiO−66-NO_2	5.0 (273 K, 9.8 bar)	2.3 (273 K, 9.8 bar)	This work

equation ($dp/p = \Delta H dT/RT2$) from isotherms that measured at 273 and 298 K. Generally, CO_2 isosteric heats of adsorption slightly reduced with increasing coverage of CO_2 on samples. UiO-66-NO_2 showed the lowest value due to a larger pore size [60]. The adsorption heat of CO_2 adsorption at different CO_2 loading on samples were found at an average between 28 and 33 kJ/mol, which are in the range of heat of adsorption of most MOFs. On the other hand, the average adsorption heat values of CH_4 at different CH_4 coverages were between 18 and 29 kJ/mol on samples. Similar to the previous work, the isosteric heat of CH_4 increased on samples with high loading of CH_4, relating to more dispersion of CH_4 occurring on the polar surface [61].

4. Conclusions

Multifunctionalized Zr-based MOFs samples (UiO-66-NO_2, UiO-66-NO_2-NH_2 10%, UiO-66-NO_2-NH_2 75%, UiO-66-NH_2, UiO-66-NH_2-NO_2 10% and UiO-66-NH_2-NO_2 75%) were obtained for CO_2 and CH_4 adsorption. ^{1}H NMR and FTIR indicate the good incorporation of the two functional groups of BDC–NO_2 and BDC–NH_2 in MOF structures. Uptake capacities of CO_2 and CH_4 on UiO-66-NH_2-NO_2 10% were the highest around 6.6 and 9.1 mmol CO_2/g at 298 and 273 K, respectively, and 2.5 and 3.5 mmol CH_4/g, at 298 and 273 K, respectively. UiO-66-NO_2-NH_2 75% presented the lowest of CO_2 and CH_4 adsorption. Overall, mixed ligands MOFs demonstrated good adsorption of CO_2 and CH_4, however, selectivity of CO_2/CH_4 could be reduced.

Acknowledgements

We thank Ms Elaine Miller for SEM measurements. We also acknowledge the Ministry of Higher Education and Minister of Natural Resources/Kurdistan regional government-Iraq for PhD scholarship. This project was supported by Australian Research Council (DP170104264).

Appendix A. Supporting information

Supplementary data associated with this article can be found in the

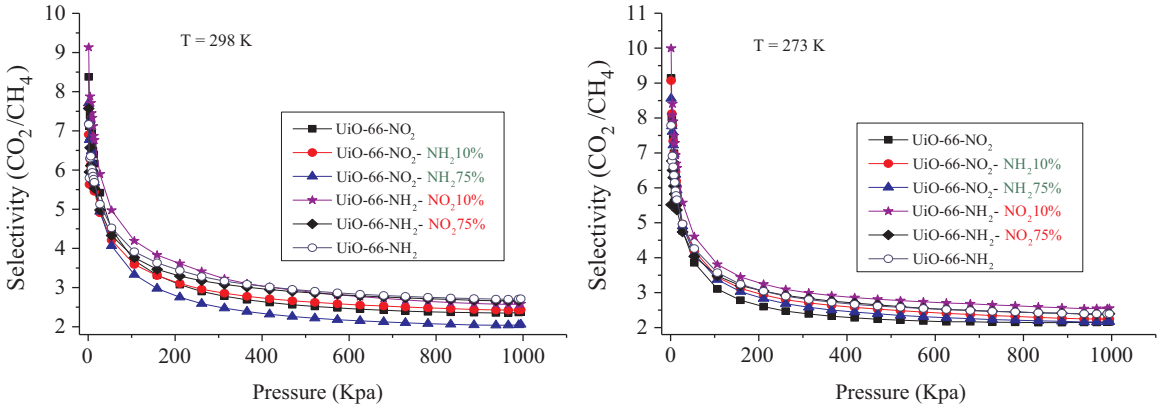

Fig. 10. Selectivity of CO_2/CH_4 of varying MOFs at 273 and 298 K.

Table 2
Separation selectivity of CO_2/CH_4 on various MOFs.

MOFs	CO_2/CH_4 at 298 K	CO_2/CH_4 at 273 K	References
UiO − 66-NH_2-NO_2 10%	4.3 (1 bar) 2.5 (9.8 bar)	3.8 (1 bar) 2.7 (9.8 bar)	This work
MIX-MIL − 125(Ti)	4.2 (1 bar) 2.9 (9.8 bar)	4.6 (1 bar) 2.6 (9.8 bar)	[32]
UiO − 66-NH_2	3.9 (1 bar) 2.7 (9.8 bar)	3.5 (1 bar) 2.3 (9.8 bar)	This work
ZIF 68	3.8 (1 bar)	5.0 (1 bar)	[59]
UiO − 66-NH_2-NO_2 75%	3.7(1 bar) 2.7 (9.8 bar)	3.4 (1 bar) 2.4 (9.8 bar)	This work
UiO − 66-NO_2	3.6 (1 bar) 2.4 (9.8 bar)	3.1 (1 bar) 2.2 (9.8 bar)	This work
UiO − 66-NO_2-NH_2 10%	3.5 (1 bar) 2.4 (9.8 bar)	3.4 (1 bar) 2.2 (9.8 bar)	This work
UiO − 66-NO_2-NH_2 75%	3.3 (1 bar) 2.0 (9.8 bar)	3.3 (1 bar) 2.2 (9.8 bar)	This work
ZIF − 69	3.4 (1 bar)	5.1 (1 bar)	[59]
ZIF − 70	3.2 (1 bar)	5.2 (1 bar)	[59]

online version at http://dx.doi.org/10.1016/j.pnsc.2018.01.016.

References

[1] P. Hu, R. Zhang, Z. Liu, H. Liu, C. Xu, X. Meng, M. Liang, S. Liang, Energy Fuels 29 (2015) 6019–6024.
[2] Z. Wang, M. Fang, H. Yu, Q. Ma, Z. Luo, Energy Fuels 27 (2013) 6887–6898.
[3] R.T. Yang, Butterworth-Heinemann, 2013.
[4] C.M. White, D.H. Smith, K.L. Jones, A.L. Goodman, S.A. Jikich, R.B. LaCount, S.B. DuBose, E. Ozdemir, B.I. Morsi, K.T. Schroeder, Energy Fuels 19 (2005) 659–724.
[5] R.V. Siriwardane, M.-S. Shen, E.P. Fisher, Energy Fuels 17 (2003) 571–576.
[6] S. Cavenati, C.A. Grande, A.E. Rodrigues, J. Chem. Eng. Data 49 (2004) 1095–1101.
[7] V. Goetz, O. Pupier, A. Guillot, Adsorption 12 (2006) 55–63.
[8] Z. Zhang, Z.-Z. Yao, S. Xiang, B. Chen, Energy Environ. Sci. 7 (2014) 2868–2899.
[9] J.-R. Li, R.J. Kuppler, H.-C. Zhou, Chem. Soc. Rev. 38 (2009) 1477–1504.
[10] Y. He, W. Zhou, G. Qian, B. Chen, Chem. Soc. Rev. 43 (2014) 5657–5678.
[11] D. Britt, H. Furukawa, B. Wang, T.G. Glover, O.M. Yaghi, Proc. Natl. Acad. Sci. USA 106 (2009) 20637–20640.
[12] H. Amrouche, S. Aguado, J. Pérez-Pellitero, C. Chizallet, F. Siperstein, D. Farrusseng, N. Bats, C. Nieto-Draghi, J. Phys. Chem. C 115 (2011) 16425–16432.
[13] J. An, S.J. Geib, N.L. Rosi, J. Am. Chem. Soc. 132 (2009) 38–39.
[14] J.A. Mason, M. Veenstra, J.R. Long, Chem. Sci. 5 (2014) 32–51.
[15] N.L. Rosi, J. Kim, M. Eddaoudi, B. Chen, M. O'Keeffe, O.M. Yaghi, J. Am. Chem. Soc. 127 (2005) 1504–1518.
[16] Y. Peng, V. Krungleviciute, I. Eryazici, J.T. Hupp, O.K. Farha, T. Yildirim, J. Am. Chem. Soc. 135 (2013) 11887–11894.
[17] H. Furukawa, N. Ko, Y.B. Go, N. Aratani, S.B. Choi, E. Choi, A.Ö. Yazaydin, R.Q. Snurr, M. O'Keeffe, J. Kim, Science 329 (2010) 424–428.
[18] S. Ma, D. Sun, J.M. Simmons, C.D. Collier, D. Yuan, H.-C. Zhou, J. Am. Chem. Soc. 130 (2008) 1012–1016.
[19] M. Lammert, S. Bernt, F. Vermoortele, D.E. De Vos, N. Stock, Inorg. Chem. 52 (2013) 8521–8528.
[20] H. Deng, C.J. Doonan, H. Furukawa, R.B. Ferreira, J. Towne, C.B. Knobler, B. Wang, O.M. Yaghi, Science 327 (2010) 846–850.
[21] Y. Yang, R. Lin, L. Ge, L. Hou, P. Bernhardt, T.E. Rufford, S. Wang, V. Rudolph, Y. Wang, Z. Zhu, Dalton Trans. 44 (2015) 8190–8197.
[22] S.S. Iremonger, R. Vaidhyanathan, R.K. Mah, G.K.H. Shimizu, Inorg. Chem. 52 (2013) 4124–4126.
[23] R. Banerjee, H. Furukawa, D. Britt, C. Knobler, M. O'Keeffe, O.M. Yaghi, J. Am. Chem. Soc. 131 (2009) 3875–3877.
[24] R.J. Kuppler, D.J. Timmons, Q.-R. Fang, J.-R. Li, T.A. Makal, M.D. Young, D. Yuan, D. Zhao, W. Zhuang, H.-C. Zhou, Coord. Chem. Rev. 253 (2009) 3042–3066.
[25] M. Eddaoudi, J. Kim, N. Rosi, D. Vodak, J. Wachter, M. O'Keeffe, O.M. Yaghi, Science 295 (2002) 469–472.
[26] Q. Yao, J. Su, O. Cheung, Q. Liu, N. Hedin, X. Zou, J. Mater. Chem. 22 (2012) 10345–10351.
[27] K. Sumida, D.L. Rogow, J.A. Mason, T.M. McDonald, E.D. Bloch, Z.R. Herm, T.-H. Bae, J.R. Long, Chem. Rev. 112 (2011) 724–781.
[28] B. Zornoza, A. Martinez-Joaristi, P. Serra-Crespo, C. Tellez, J. Coronas, J. Gascon, F. Kapteijn, Chem. Commun. 47 (2011) 9522–9524.
[29] S. Orefuwa, E. Iriowen, H. Yang, B. Wakefield, A. Goudy, Microporous Mesoporous Mater. 177 (2013) 82–90.
[30] A.D. Burrows, CrystEngComm 13 (2011) 3623–3642.
[31] H. Reinsch, S. Waitschat, N. Stock, Dalton Trans. 42 (2013) 4840–4847.
[32] Z.H. Rada, H.R. Abid, J. Shang, Y. He, P. Webley, S. Liu, H. Sun, S. Wang, Fuel 160 (2015) 318–327.
[33] S.M. Chavan, G.C. Shearer, S. Svelle, U. Olsbye, F. Bonino, J. Ethiraj, K.P. Lillerud, S. Bordiga, Inorg. Chem. 53 (2014) 9509–9515.
[34] M. Kim, J.F. Cahill, K.A. Prather, S.M. Cohen, Chem. Commun. 47 (2011) 7629–7631.
[35] Z.H. Rada, H.R. Abid, H. Sun, S. Wang, J. Chem. Eng. Data 60 (2015) 2152–2161.
[36] J.H. Cavka, S. Jakobsen, U. Olsbye, N. Guillou, C. Lamberti, S. Bordiga, K.P. Lillerud, J. Am. Chem. Soc. 130 (2008) 13850–13851.
[37] F. Vermoortele, R. Ameloot, A. Vimont, C. Serre, D. De Vos, Chem. Commun. 47 (2011) 1521–1523.
[38] S.J. Garibay, S.M. Cohen, Chem. Commun. 46 (2010) 7700–7702.
[39] T. Devic, P. Horcajada, C. Serre, F. Salles, G. Maurin, B. Moulin, D. Heurtaux, G. Clet, A. Vimont, J.-M. Greneche, J. Am. Chem. Soc. 132 (2009) 1127–1136.
[40] H. Muckenhuber, H. Grothe, Carbon 44 (2006) 546–559.
[41] S.A. Boyd, G. Sheng, B.J. Teppen, C.T. Johnston, Environ. Sci. Technol. 35 (2001) 4227–4234.
[42] H.R. Abid, G.H. Pham, H.-M. Ang, M.O. Tade, S. Wang, J. Colloid Interface Sci. 366 (2012) 120–124.
[43] X. Kong, H. Deng, F. Yan, J. Kim, J.A. Swisher, B. Smit, O.M. Yaghi, J.A. Reimer, Science 341 (2013) 882–885.
[44] M. Kandiah, M.H. Nilsen, S. Usseglio, S. Jakobsen, U. Olsbye, M. Tilset, C. Larabi, E.A. Quadrelli, F. Bonino, K.P. Lillerud, Chem. Mater. 22 (2010) 6632–6640.
[45] H. Frost, T. Düren, R.Q. Snurr, J. Phys. Chem. B 110 (2006) 9565–9570.
[46] H.R. Abid, H.M. Ang, S. Wang, Nanoscale 4 (2012) 3089–3094.
[47] F. Vermoortele, M. Vandichel, B. Van de Voorde, R. Ameloot, M. Waroquier, V. Van Speybroeck, D.E. De Vos, Angew. Chem. Int. Ed. 51 (2012) 4887–4890.
[48] Z. Hu, Y. Peng, Z. Kang, Y. Qian, D. Zhao, Inorg. Chem. 54 (2015) 4862–4868.
[49] M. Abu Ghalia, Y. Dahman, Energy Technol. 5 (2017) 356–372.
[50] A. Phan, C.J. Doonan, F.J. Uribe-Romo, C.B. Knobler, M. O'Keeffe, O.M. Yaghi, Acc. Chem. Res. 43 (2010) 58–67.
[51] Z.H. Rada, H.R. Abid, J. Shang, Y. He, P. Webley, S. Liu, H. Sun, S. Wang, Fuel 160 (2015) 318–327.
[52] C. Volkringer, T. Loiseau, M. Haouas, F. Taulelle, D. Popov, M. Burghammer, C. Riekel, C. Zlotea, F. Cuevas, M. Latroche, D. Phanon, C. Knöfelv, P.L. Llewellyn, G. Férey, Chem. Mater. 21 (2009) 5783–5791.
[53] C.A. Fernandez, P.K. Thallapally, R.K. Motkuri, S.K. Nune, J.C. Sumrak, J. Tian, J. Liu, Cryst. Growth Des. 10 (2010) 1037–1039.
[54] Z. Liang, M. Marshall, A.L. Chaffee, Energy Fuels 23 (2009) 2785–2789.
[55] S. Bourrelly, P.L. Llewellyn, C. Serre, F. Millange, T. Loiseau, G. Férey, J. Am. Chem. Soc. 127 (2005) 13519–13521.
[56] D.K. Maity, A. Halder, B. Bhattacharya, A. Das, D. Ghoshal, Cryst. Growth Des. 16 (2016) 1162–1167.
[57] J.A. Mason, K. Sumida, Z.R. Herm, R. Krishna, J.R. Long, Energy Environ. Sci. 4

(2011) 3030–3040.
[58] S.S. Iremonger, R. Vaidhyanathan, R.K. Mah, G.K. Shimizu, Inorg. Chem. 52 (2013) 4124–4126.
[59] A. Phan, C.J. Doonan, F.J. Uribe-Romo, C.B. Knobler, M. O'keeffe, O.M. Yaghi, Acc. Chem. Res 43 (2010) 58–67.
[60] P.I. Ravikovitch, A. Vishnyakov, R. Russo, A.V. Neimark, Langmuir 16 (2000) 2311–2320.
[61] Z.H. Rada, H.R. Abid, J. Shang, H. Sun, Y. He, P.A. Webley, S. Liu, S. Wang, Ind. Eng. Chem. Res. 55 (2016) 7924–7932.